ATLAS NOTE

ATLAS-CONF-2013-035

March 24, 2013

Search for direct production of charginos and neutralinos in events with three leptons and missing transverse momentum in 21 fb^{-1} of pp collisions at $\sqrt{s}$ = 8 TeV with the ATLAS detector

The ATLAS Collaboration

Abstract

A search for the direct production of charginos and neutralinos in final states with three leptons (electrons or muons) and missing transverse momentum is presented. The analysis is based on 20.7 fb^{-1} of proton-proton collision data delivered by the LHC at $\sqrt{s} = 8$ TeV and recorded by the ATLAS detector. No excess above the Standard Model expectation is observed in six signal regions that are either enriched or depleted in Z-boson decays. Limits are placed at the 95% confidence level on the masses of the charginos and neutralinos in simplified supersymmetric models. Chargino and heavy neutralino masses are excluded up to 600 GeV if these particles decay through sleptons and up to 315 GeV if they decay via gauge bosons to a massless lightest neutralino.

ATLAS-CONF-2013-035
26 March 2013

1 Introduction

Supersymmetry (SUSY) [1–9] postulates the existence of SUSY particles, or "sparticles", with spin differing by one-half unit with respect to that of their Standard Model (SM) partner. If R-parity [10–14] is conserved, sparticles can only be pair-produced and each decays into final states with SM particles and the lightest SUSY particle (LSP) which is stable. Charginos ($\tilde{\chi}_i^{\pm}$, $i = 1, 2$) and neutralinos ($\tilde{\chi}_j^0$, $j = 1, 2, 3, 4$), are the mass eigenstates formed from the linear superposition of the SUSY partners of the Higgs and electroweak gauge bosons. Naturalness suggests the lightest $\tilde{\chi}_i^{\pm}$ and $\tilde{\chi}_j^0$ (and third-generation squarks) have masses in the hundreds of GeV range [15, 16]. In scenarios where the masses of the first two generations of squarks and the gluino are larger than a few TeV, the direct production of charginos and neutralinos may be the dominant SUSY processes at the Large Hadron Collider (LHC). Charginos can decay into leptonic final states via sneutrinos ($\tilde{\chi}_{1,2}^{\pm} \to \tilde{\nu}\ell^{\pm} \to \tilde{\chi}_1^0 \nu\ell^{\pm}$), charged sleptons (denoted sleptons in the following) ($\tilde{\chi}_{1,2}^{\pm} \to \tilde{\ell}^{\pm}\nu \to \tilde{\chi}_1^0 \ell^{\pm}\nu$) or W-bosons ($\tilde{\chi}_{1,2}^{\pm} \to W^{\pm}\tilde{\chi}_1^0 \to \ell^{\pm}\nu\tilde{\chi}_1^0$), while heavy neutralinos can decay via sleptons ($\tilde{\chi}_{2,3,4}^0 \to \ell^{\pm}\tilde{\ell}^{\mp} \to \ell^{\pm}\ell^{\mp}\tilde{\chi}_1^0$), Z-bosons ($\tilde{\chi}_{2,3,4}^0 \to Z\tilde{\chi}_1^0 \to \ell^{\pm}\ell^{\mp}\tilde{\chi}_1^0$) or Higgs bosons ($\tilde{\chi}_{2,3,4}^0 \to h\tilde{\chi}_1^0 \to \ell^{\pm}\ell^{\mp}\tilde{\chi}_1^0 + X$, where X represents possible additional decay products of the Higgs boson).

This note presents a search with the ATLAS detector for the direct production of charginos and neutralinos decaying to a final state with three leptons (electrons or muons) and missing transverse momentum, the latter originating from the two undetected LSPs and the neutrinos. The analysis is based on 20.7 fb^{-1} of proton-proton collision data recorded by ATLAS at a centre-of-mass energy of $\sqrt{s} = 8$ TeV.

The results are interpreted in simplified supersymmetric models ("simplified models" [17]) for the associate production of $\tilde{\chi}_1^{\pm}$ and $\tilde{\chi}_2^0$, where the masses and the decay modes of the relevant particles ($\tilde{\chi}_1^{\pm}$, $\tilde{\chi}_1^0$, $\tilde{\chi}_2^0$, $\tilde{\nu}$, $\tilde{\ell}_{\mathrm{L}}$) are the only free parameters. It is assumed that the $\tilde{\chi}_1^{\pm}$ and $\tilde{\chi}_2^0$ consist predominantly of the wino component and are mass degenerate, while the $\tilde{\chi}_1^0$ consists predominantly of the bino component. Two different scenarios for the decay of the $\tilde{\chi}_1^{\pm}$ and $\tilde{\chi}_2^0$ are considered, where in both cases the decays are prompt. In the first scenario, the $\tilde{\chi}_1^{\pm}$ and $\tilde{\chi}_2^0$ decay with a branching fraction of 1/6 through $\tilde{e}_L$, $\tilde{\mu}_L$, $\tilde{\tau}_L$, $\tilde{\nu}_e$, $\tilde{\nu}_\mu$, and $\tilde{\nu}_\tau$ with masses $m_{\tilde{\nu}} = m_{\tilde{\ell}_L} = (m_{\tilde{\chi}_1^0} + m_{\tilde{\chi}_1^{\pm}})/2$. In the second scenario, all sleptons are assumed to be very heavy so that the $\tilde{\chi}_1^{\pm}$ and $\tilde{\chi}_2^0$ decay via W and Z-bosons that may be on or off mass-shell. In the simplified models of this analysis, the branching ratios for decays via the Higgs bosons are set to zero. Diagrams for the considered $\tilde{\chi}_1^{\pm}\tilde{\chi}_2^0$ production and decay to final states with three leptons are shown in Figure 1.

Previous searches for these processes are documented in Refs. [18–21] by ATLAS, and in Ref. [22] by CMS. Similar searches have been conducted at the Tevatron [23, 24]. At LEP [25], searches for direct chargino production have set a model-independent lower limit of 103.5 GeV at 95% confidence level (CL) on the mass of promptly decaying charginos.

2 Detector Description

The ATLAS detector [26] is a multi-purpose particle physics detector with forward-backward symmetric cylindrical geometry[1]. The inner tracking detector (ID) covers $|\eta| < 2.5$ and consists of a silicon pixel detector, a silicon micro-strip detector, and a transition radiation tracker. The ID is surrounded by a thin superconducting solenoid providing a 2 T axial magnetic field. A high-granularity lead/liquid-argon (LAr) sampling calorimeter measures the energy and the position of electromagnetic showers within $|\eta| <$

[1] ATLAS uses a right-handed coordinate system with its origin at the nominal interaction point (IP) in the centre of the detector and the z-axis along the beam pipe. The x-axis points from the IP to the centre of the LHC ring, and the y-axis points upward. Cylindrical coordinates (r, ϕ) are used in the transverse plane, ϕ being the azimuthal angle around the beam pipe. The pseudorapidity is defined in terms of the polar angle θ as $\eta = -\ln\tan(\theta/2)$.

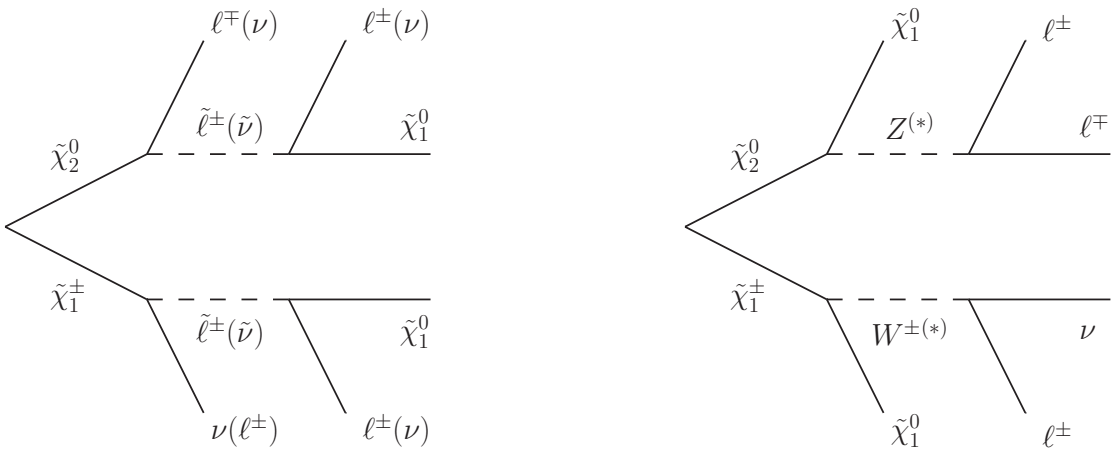

(a) via sleptons (b) via gauge bosons

Figure 1: Illustration of $\tilde{\chi}_1^{\pm}\tilde{\chi}_2^0$ production and decay to three lepton final states.

3.2. LAr sampling calorimeters are also used to measure hadronic showers in the end-cap ($1.5 < |\eta| < 3.2$) and forward ($3.1 < |\eta| < 4.9$) regions, while an iron-scintillator tile calorimeter measures hadronic showers in the central region ($|\eta| < 1.7$). The muon spectrometer surrounds the calorimeters and consists of three large superconducting air-core toroid magnets, each with eight coils, a system of precision tracking chambers ($|\eta| < 2.7$), and fast trigger chambers. A three-level trigger system [27] selects events to be recorded for offline analysis.

3 Monte Carlo simulation

Several Monte Carlo (MC) generators are used to simulate SM processes and new physics signals relevant for this analysis. SHERPA [28] is used to simulate the diboson processes WW, WZ and ZZ, where "Z" also includes virtual photons. These diboson samples correspond to all SM diboson diagrams leading to the $\ell\nu\ell'\nu'$, $\ell\ell\ell'\nu'$, and $\ell\ell\ell'\ell'$ final states, where $\ell, \ell' = e, \mu, \tau$ and $\nu, \nu' = \nu_e, \nu_\mu, \nu_\tau$. Interference between the diagrams is taken into account. ALPGEN [29] is used for the $t\bar{t}W$, $t\bar{t}Z$ processes and MadGraph [30] is chosen for the $t\bar{t}WW$ process. The triboson processes, WWW and ZWW are also simulated using MadGraph. POWHEG [31] is chosen for the simulation of the pair production of top quarks ($t\bar{t}$), ACERMC [32] is used for the simulation of the t-channel, while MC@NLO [33] for the other single top production processes, and ALPGEN is used to simulate W+jets and Z+jets processes. Additional samples are produced using the POWHEG generator to assess systematic uncertainties related to the choice of MC generator for the WZ and ZZ processes.

The choice of the parton distribution functions (PDF) depends on the generator. The CTEQ6L1 [34] PDFs are used with MadGraph and ALPGEN, and the CT10 [35] PDFs with MC@NLO and SHERPA. Fragmentation and hadronisation for the ALPGEN and MC@NLO samples are performed with HERWIG [36]. For MadGraph, POWHEG and ALPGEN single vector boson samples PYTHIA [37] is used instead. For SHERPA samples, the fragmentation and hadronisation is performed internally. JIMMY [38] is interfaced to HERWIG for simulation of the underlying event.

For all MC samples, the propagation of particles through the ATLAS detector is modelled with GEANT4 [39] using the full ATLAS detector simulation [40] (except the $t\bar{t}$ POWHEG sample which uses fast detector simulation AtlFast-II [41]). The effect of multiple proton-proton collisions from the same or different beam bunch crossings (pile-up) is incorporated into the simulation by overlaying additional minimum-bias events generated with PYTHIA onto hard-scatter events. Simulated events are weighted

to match the distribution of the number of interactions per bunch crossing observed in data, but are otherwise reconstructed in the same manner as data.

Expected diboson yields are normalised using NLO QCD predictions obtained with MCFM [42, 43]. Triboson contributions are also normalised to NLO predictions [44]. The top-quark pair-production contribution is normalised to approximate next-to-next-to-leading-order calculations (NNLO) [45] and the $t\bar{t}W$, $t\bar{t}WW$, $t\bar{t}Z$ contributions are normalised to NLO predictions [46, 47]. The theoretical cross-sections for W+jets and Z+jets are calculated with DYNNLO [48] with the MSTW 2008 NNLO [49] PDF set.

The simplified model signal samples are produced with Herwig++ [50] using the CTEQ6L1 PDF set. The cross-sections are calculated to next-to-leading order in the strong coupling constant using PROSPINO2 [51]. The nominal cross-section and the uncertainty are taken from an envelope of cross-section predictions using different PDF sets and factorisation and renormalisation scales, as described in Ref. [52].

4 Event Reconstruction and Preselection

The data sample was collected with an inclusive selection of single and double electron/muon triggers with asymmetric and symmetric transverse momentum (p_{T}) thresholds. For events that are selected by the single electron or single muon triggers, at least one signal electron or muon is required to have $p_{\mathrm{T}} > 25$ GeV. For events that are selected by the symmetric di-muon trigger, at least two signal muons are required to have $p_{\mathrm{T}} > 14$ GeV, while for the asymmetric trigger the requirements are $p_{\mathrm{T}} > 18$ GeV and $p_{\mathrm{T}} > 10$ GeV. In the case of the symmetric di-electron trigger, at least two signal electrons are required to have $p_{\mathrm{T}} > 14$ GeV, while for the asymmetric electron trigger the requirements are $p_{\mathrm{T}} > 25$ GeV and $p_{\mathrm{T}} > 10$ GeV. For events that are selected using the electron-muon (muon-electron) trigger, at least one signal electron is required to have $p_{\mathrm{T}} > 14$ GeV (10 GeV) and at least one signal muon to have $p_{\mathrm{T}} > 10$ GeV (18 GeV). These thresholds are chosen such that the overall fiducial trigger efficiency is high, typically in excess of 90%, and independent of the transverse momentum of the triggerable objects within uncertainties. The trigger requirements and corresponding offline selection cuts are placed in both data and MC simulation.

Events recorded during normal running conditions are analysed if the reconstructed primary vertex has five or more tracks associated with it. The primary vertex of an event is identified as the vertex with the highest Σp_{T}^2 of associated tracks.

Electrons must satisfy "medium" identification criteria [53] and fulfill $p_{\mathrm{T}} > 10\,\mathrm{GeV}$ and $|\eta| < 2.47$, where p_{T} and η are determined from the calibrated clustered energy deposits in the electromagnetic calorimeter and the matched ID track, respectively. Muons are reconstructed by combining tracks in the ID and tracks in the muon spectrometer [54]. Reconstructed muons are considered as candidates if they have transverse momentum $p_{\mathrm{T}} > 10\,\mathrm{GeV}$ and $|\eta| < 2.4$.

Jets are reconstructed with the anti-k_t algorithm [55] with a radius parameter of $R = 0.4$ using topological clusters [56]. The clusters are calibrated using a local cluster calibration [27], which involves weighting differently the energy deposits arising from electromagnetic showers and those from hadronic showers. The final jet energy calibration includes the jet energy scale [57], which corrects the calorimeter response to the jet energy at particle level. The correction factors were obtained from simulation and have been refined and validated using data. Jets considered in this analysis have $p_{\mathrm{T}} > 20\,\mathrm{GeV}$ and $|\eta| < 2.5$. For jets with tracks, the p_{T}-weighted fraction of the tracks in the jet that are associated with the primary vertex is required to be larger than 0.5. Events containing jets failing the quality criteria described in Ref. [57] are rejected to suppress both SM and beam-induced backgrounds. Jets are identified as containing b-hadron decays, and thus called "b-jets", using a multivariate technique based on quantities such as the impact parameters of the tracks associated with the jet. The chosen working point of the b-tagging

algorithm [58] correctly identifies b-jets in simulated top-quark decays with an efficiency of 85% and misidentifies light-flavour jets with a rate of about 10% for jets with $p_{\mathrm{T}} > 20\,\mathrm{GeV}$ and $|\eta| < 2.5$ [59].

The missing transverse momentum, $E_{\mathrm{T}}^{\mathrm{miss}}$, is the magnitude of the vector sum of the transverse momentum or transverse energy of all $p_{\mathrm{T}} > 10\,\mathrm{GeV}$ muons, $p_{\mathrm{T}} > 10\,\mathrm{GeV}$ electrons, $p_{\mathrm{T}} > 20\,\mathrm{GeV}$ jets, and calibrated calorimeter energy clusters with $|\eta| < 4.9$ not associated with these objects.

In this analysis, "tagged" leptons are leptons separated from each other and from candidate jets as described below. If two candidate electrons are reconstructed with $\Delta R \equiv \sqrt{(\Delta\phi)^2 + (\Delta\eta)^2} < 0.1$, the lower energy one is discarded. Candidate jets within $\Delta R = 0.2$ of an electron candidate are rejected. To suppress leptons originating from semi-leptonic decays of c- and b-quarks, all lepton candidates are required to be separated from candidate jets by $\Delta R > 0.4$. Muons undergoing bremsstrahlung can be reconstructed with an overlapping electron candidate. To reject these, tagged electrons and muons separated from jets and reconstructed within $\Delta R = 0.1$ of each other are both discarded. Events containing one or more tagged muons that have transverse impact parameter with respect to the primary vertex $|d_0| > 0.2\,\mathrm{mm}$ or longitudinal impact parameter with respect to the primary vertex $|z_0| > 1\,\mathrm{mm}$ are rejected to suppress cosmic muon background.

"Signal" leptons are tagged leptons that are required to be isolated: the scalar sum of the transverse momenta of tracks within a cone of $\Delta R = 0.3$ around the lepton candidate, and excluding the lepton candidate track itself, must be less than 16% (12%) of the lepton p_{T} for electrons (muons). Tracks selected for the electron (muon) isolation requirement defined above are those which have $p_{\mathrm{T}} > 0.4$ (1.0) GeV and are associated with the primary vertex of the event. Contributions from the tracks of other tagged electrons or muons are subtracted. To suppress leptons originating from secondary vertices, the distance of closest approach of the lepton track to the primary vertex normalised to its uncertainty is required to satisfy $|d_0|/\sigma(d_0) < 5\,(3)$, and $|z_0 \sin\theta|$ is chosen to be less than 0.4 (1) mm for electrons (muons). Signal electrons must also pass "tight" identification criteria [53] and the sum of the energy deposits in the calorimeter (corrected for pile-up effects) within a cone of $\Delta R = 0.3$ around the electron candidate is required to be less than 18% of the electron p_{T}.

5 Signal Region Selection

Selected events must contain exactly three signal leptons. As the decays of $\tilde{\chi}_j^0$ through sleptons or Z-bosons yield same-flavour opposite-sign (SFOS) lepton pairs, the presence of at least one such pair is required. The invariant mass of any SFOS lepton pair must be above 12 GeV to suppress background from low-mass resonances. Events are further required not to contain any b-jets with $p_{\mathrm{T}} > 20\,\mathrm{GeV}$ to suppress contributions from top quark production.

Six signal regions are then defined: three "Z-depleted" regions ("SRnoZa", "SRnoZb" and "SRnoZc"), with no SFOS pairs having an invariant mass within 10 GeV of the Z-boson mass; and three "Z-enriched" regions ("SRZa", "SRZb" and "SRZc"), where at least one SFOS pair has an invariant mass within 10 GeV of the Z-boson mass. The Z-depleted regions target neutralino decays via intermediate sleptons or via off-shell Z-bosons while the Z-enriched regions target decays via an on-shell Z-boson.

"Loose", "medium" and "tight" signal regions are defined for the Z-depleted and Z-rich regions. The loose regions (SRnoZa and SRZa) are defined with an intermediate $E_{\mathrm{T}}^{\mathrm{miss}}$ requirement. SRnoZa targets scenarios with small mass splitting between the lightest neutralinos, while the medium signal region SRnoZb targets scenarios with mass splitting just below that of the Z-boson mass. The tight signal region SRnoZc is designed to increase sensitivity to scenarios characterised by large mass splittings between the lightest neutralinos by requiring the third-leading lepton to have $p_{\mathrm{T}} > 30\,\mathrm{GeV}$. Events in SRnoZa and SRnoZb are also required not to pass the SRnoZc selection so that these regions remain orthogonal. In the tighter signal regions, the transverse mass variable $m_{\mathrm{T}} = \sqrt{2 \cdot E_{\mathrm{T}}^{\mathrm{miss}} \cdot p_{\mathrm{T}}^{\ell} \cdot (1 - \cos\Delta\phi_{\ell, E_{\mathrm{T}}^{\mathrm{miss}}})}$ must be

Table 1: The selection requirements for the signal regions. All regions are mutually exclusive and require exactly three signal leptons and a same-flavour opposite-sign (SFOS) lepton pair. Events with a b-jet or a SFOS lepton pair with mass less than 12 GeV are rejected. The mass of the SFOS lepton pair closest to the Z-boson mass is denoted by m_{SFOS}. The m_{T} is calculated from the $E_{\text{T}}^{\text{miss}}$ and the lepton not forming the SFOS lepton pair closest to the Z-boson mass.

Selection	SRnoZa	SRnoZb	SRnoZc	SRZa	SRZb	SRZc
m_{SFOS} [GeV]	<60	60–81.2	<81.2 or >101.2	81.2–101.2	81.2–101.2	81.2–101.2
$E_{\text{T}}^{\text{miss}}$ [GeV]	>50	>75	>75	75–120	75–120	>120
m_{T} [GeV]	–	–	>110	<110	>110	>110
p_{T} 3$^{\text{rd}}$ ℓ [GeV]	>10	>10	>30	>10	>10	>10
SR veto	SRnoZc	SRnoZc	–	–	–	–

above 110 GeV, where the lepton entering the m_{T} calculation is the one which is not included in the SFOS lepton pair with invariant mass closest to the Z-boson mass. The m_{T} requirement is introduced to suppress background from WZ events, as events with $W \to \ell\nu$ decays are characterised as having $m_{\text{T}} \lesssim m_W$. In SRZc, the $E_{\text{T}}^{\text{miss}}$ requirement is raised to 120 GeV to further suppress the WZ background. There is no requirement on the number of non-b-jets in any signal region. Table 1 summarises the selection requirements for the signal regions.

6 Standard Model Background Estimation

Several SM processes contribute to the background in the signal regions. A background process is considered "irreducible" if it leads to events with three real and isolated prompt leptons, referred to as "real" leptons below. A "reducible" process has at least one "fake" object, that is either a lepton from a semileptonic decay of a heavy-flavour quark, a lepton from a misidentified light flavour quark or gluon jet, referred to as "light flavour", or an electron from a photon conversion.

6.1 Reducible Background Processes

The reducible background includes single- and pair-production of top quarks, WW and single W or Z-boson processes produced in association with jets or photons. The dominant component is the production of top quarks, followed by Z+jets. The reducible background is estimated using a "matrix method" similar to that described in Ref. [60] and which has been previously used in Refs. [18, 19, 21].

In this implementation of the matrix method, the signal lepton with the highest p_{T} is taken to be real, which is a valid assumption in 99% of three lepton events, based on simulation. The number of observed events with one or two fake leptons is then extracted from a system of linear equations relating the number of events with two additional signal or tagged candidates to the number of events with two additional candidates that are either real or fake. The coefficients of the linear equations are functions of the real-lepton identification efficiencies and of the fake-object misidentification probabilities.

The real identification efficiencies are obtained from MC simulation in the region of interest and are scaled by correction factors to account for potential differences with respect to data. The real lepton efficiency correction factors are obtained in a control region enriched in $Z \to e^+e^-$ and $Z \to \mu^+\mu^-$ decays and are found to be 0.99 ± 0.01 for both electrons and muons.

Misidentification probabilities for each relevant fake type (light flavour, heavy flavour or conversion) and for each reducible background process, parameterised with the lepton p_{T} and η, are obtained using simulated events with one signal and two tagged leptons. These misidentification probabilities are then

corrected using the ratio ("fake correction factor") of the misidentification probability in data to that in simulation obtained from dedicated control samples. The fake correction factors are assumed to be independent of selected regions and any potential composition or kinematic differences. Systematic uncertainties are included to describe the accuracy of this assumption (Section 7) and the validity of the assumption is confirmed by the agreement in the validation regions presented in Section 8. The occurrence of light flavour fake leptons is rare compared to other types and the correction factor is assumed to be 1.

For heavy-flavour fakes, the correction factor is measured in a $b\bar{b}$-dominated control sample. This is defined by selecting events with only one b-jet (containing a muon) and a tagged lepton, for which the fake rate is measured. Contaminating backgrounds leading to the production of real leptons from W decays include top-quark pair-production and W bosons produced in association with b-jets. A requirement that $E_{\mathrm{T}}^{\mathrm{miss}}$ be less than 60 GeV suppresses both the $t\bar{t}$ and the W contamination, and requiring $m_{\mathrm{T}} < 50$ GeV (constructed using the tagged lepton) further reduces the W background. The remaining (∼1% level) background is subtracted from data using MC predictions. The heavy flavour fake correction factor is found to be 0.75 ± 0.04 (0.86 ± 0.03) for electrons (muons).

The fake correction factor for the conversion candidates is determined in a sample of photons radiated from a muon in $Z \to \mu\mu$ decays. These are selected by requiring $m_{\mu\mu e}$ to lie within 10 GeV of the Z-boson mass. The conversion fake correction factor for electrons is found to be 1.22 ± 0.27.

A weighted average misidentification probability is then calculated by weighting the corrected type- and process-dependent misidentification probabilities according to their relative contributions in a given signal or validation region, defined below.

6.2 Irreducible Background Processes

Irreducible processes include diboson (WZ and ZZ), triboson (WWW, ZZZ and ZWW) and $t\bar{t}W/Z$ production, where the gauge bosons may be on or off mass shell. The WZ, ZZ, triboson, and $t\bar{t}W/Z$ contributions are determined using the corresponding MC samples, for which lepton and b-jet selection efficiencies are corrected to account for differences with respect to data. The MC simulation of the irreducible processes, particularly WZ, is checked in multiple validation regions and is seen to agree well with data (see Section 8).

In the previous preliminary result by ATLAS in Ref. [18], the WZ contribution was determined using a semi-data-driven approach. The WZ background was fitted to data in a control region, with a normalisation factor consistent with unity. When setting limits on specific new physics scenarios, the signal contamination in the WZ control region was taken into account. This approach led to reduced sensitivity to some scenarios that gave sizeable contamination in the WZ control region – even if the corresponding yields in the signal regions were very large. To maximise sensitivity to new physics scenarios, the normalisation of the WZ contribution is set to the `MCFM` predictions.

7 Systematic uncertainties

Several sources of systematic uncertainty are considered for the SM background estimates and signal yield predictions. The systematic uncertainties affecting the simulation-based estimates (the yield of the irreducible background, the cross-section weighted misidentification probabilities, and the signal yield) include the theoretical cross-section uncertainties due to the choice of renormalisation and factorisation scale and PDFs, the acceptance uncertainty due to PDFs, the choice of MC generator, the uncertainty on the luminosity, the uncertainty due to the jet energy scale, jet energy resolution, lepton energy scale, lepton energy resolution, lepton identification efficiency, $E_{\mathrm{T}}^{\mathrm{miss}}$ energy scale and resolution, and the uncertainty due to b-tagging efficiency and mistag probability. The systematic uncertainty associated with

the simulation of pile-up (∼10%) is also taken into account. The theoretical cross-section uncertainties for the non-WZ irreducible backgrounds used in this analysis are 30% for $t\bar{t}$ + $W/Z/WW$ [46, 47] and 5% for ZZ. A 100% uncertainty is assumed on the triboson contribution. The uncertainty on the WZ yield, 12%, is obtained from the difference between the MCFM based cross-section and the ATLAS measured cross-section (8%) added in quadrature with the quoted uncertainty on the ATLAS measurement (9%) [61].

In SRnoZa (b and c), the total uncertainty on the irreducible background is 14% (17% and 33%). This is dominated by the uncertainties on the cross-sections, the jet energy resolution and the $E_{\mathrm{T}}^{\mathrm{miss}}$ energy scale (∼ 7–15% each). All the remaining uncertainties on the irreducible background in these signal regions are below 5%. In SRZa (b and c), the total uncertainty on the irreducible background is similar: 13% (24% and 21%). In the SRZ regions, the uncertainty on the WZ acceptance due to the choice of MC generator (10–12%), determined by comparing the SHERPA and POWHEG estimates, and the uncertainty on the cross-sections listed above dominate the total uncertainty. The uncertainty from the limited number of simulated events in the tight signal regions SRnoZc and SRZc is ∼14%.

The uncertainty on the reducible background includes the MC uncertainty on the weights for the misidentification probabilities from the sources listed in Section 6.1 (up to 10%) and the uncertainty due to the dependence of the misidentification probability on $E_{\mathrm{T}}^{\mathrm{miss}}$ (0.5–20%). Also included in the uncertainty on the reducible background is the uncertainty on the fake correction factors (5-8%). In SRnoZa and SRnoZb, the uncertainty on the reducible background is dominated by the uncertainty due to the dependence of the misidentification probability on $E_{\mathrm{T}}^{\mathrm{miss}}$ and is ∼40% in SRnoZa and ∼60% in SRnoZb. In SRnoZc, the uncertainty on the reducible background is dominated by the statistical uncertainty from the limited number of data events with three tagged leptons, of which at least one is a signal lepton, and it is ∼40% (∼7% in SRnoZa and ∼12% in SRnoZb). The same source also dominates the uncertainty on the reducible background component in SRZa, SRZb and SRZc, where it is ∼35%, ∼35% and ∼70% respectively.

The uncertainties on the signal yields from experimental sources range from 5–20% and are dominated by the uncertainty on the electron energy scale, the jet energy scale and the $E_{\mathrm{T}}^{\mathrm{miss}}$ energy scale and resolution. The uncertainties from theoretical sources range from 5–10% and are dominated by the uncertainty on the cross-sections.

For the 2012 data set the preliminary uncertainty on the luminosity is 3.6% based on the calibration procedure described in Ref. [62]. A 5% uncertainty is applied to MC samples to cover differences in efficiency seen between the trigger in data and the MC trigger simulation. Correlations of systematic uncertainties between processes and regions are taken into account.

8 Background Model Validation

The background predictions have been tested in validation regions that are defined to be close, albeit orthogonal, to the signal region selections. For both types of signal regions, with and without a Z candidate, two validation regions are defined that target different background processes. One requires low $E_{\mathrm{T}}^{\mathrm{miss}}$ and no b-jet requirement and it is dominated by the Drell-Yan process (VRnoZa and VRZa); the other one selects events with high $E_{\mathrm{T}}^{\mathrm{miss}}$ while requesting at least one b-jet and it is enriched in top production processes (VRnoZb and VRZb). All validation regions select exactly three leptons and a SFOS lepton pair. Table 2 summarises the selection requirements. Validation region VRnoZa is dominated by WZ^*, Z^*Z^* and Z^*+jets processes where the Z-bosons are off-shell. Top pair production dominates VRnoZb. The main contributions in region VRZa are from WZ and Z+jets, while WZ is dominant in VRZb.

In the validation regions, the data and SM expectation are in agreement within statistical and systematic uncertainties as shown in Table 3. The m_{T}, number of b-jets, m_{SFOS}, and third lepton p_{T} distributions in VRnoZa are shown in Figure 2, while the m_{T} and number of b-jets in VRZa are plotted in Figure 3.

Figure 4 shows the m_{T}, $E_{\mathrm{T}}^{\mathrm{miss}}$, m_{SFOS}, and third lepton p_{T} distributions in VRnoZb and Figure 5 shows the distributions of m_{T} and $E_{\mathrm{T}}^{\mathrm{miss}}$.

Table 2: The selection requirements of the validation regions. All regions require exactly three signal leptons and a same-flavour opposite-sign (SFOS) lepton pair. Events that contain a SFOS lepton pair with a mass less than 12 GeV are rejected. The mass of the SFOS lepton pair closest to the Z-boson mass is denoted by m_{SFOS}.

Selection	VRnoZa	VRnoZb	VRZa	VRZb
m_{SFOS} [GeV]	<81.2 or >101.2	<81.2 or >101.2	81.2–101.2	81.2–101.2
b-jet	veto	request	veto	request
$E_{\mathrm{T}}^{\mathrm{miss}}$ [GeV]	35–50	>50	30–50	>50
Dominant process	WZ^*, Z^*Z^*, Z^*+jets	$t\bar{t}$	WZ, Z+jets	WZ

Table 3: Expected numbers of events in the validation regions from SM backgrounds and observed numbers of events in data for 20.7 fb^{-1}. Both statistical and systematic uncertainties are included.

Selection	VRnoZa	VRnoZb	VRZa	VRZb
Tri-boson	1.4 ± 1.4	0.5 ± 0.5	0.6 ± 0.6	0.26 ± 0.26
ZZ	$(1.3 \pm 0.9) \times 10^2$	4.5 ± 2.8	108 ± 23	6.9 ± 2.2
$t\bar{t}V$	2.9 ± 1.2	21 ± 7	7.4 ± 2.6	26 ± 8
WZ	110 ± 21	34 ± 15	$(5.5 \pm 0.9) \times 10^2$	$(1.4 \pm 0.4) \times 10^2$
Σ SM irreducible	$(2.4 \pm 0.9) \times 10^2$	60 ± 16	$(6.6 \pm 0.9) \times 10^2$	$(1.7 \pm 0.4) \times 10^2$
SM reducible	$(1.5 \pm 0.6) \times 10^2$	$(0.7 \pm 0.4) \times 10^2$	$(3.8 \pm 1.4) \times 10^2$	27 ± 13
Σ SM	$(3.9 \pm 1.1) \times 10^2$	$(1.3 \pm 0.5) \times 10^2$	$(10.4 \pm 1.7) \times 10^2$	$(2.0 \pm 0.4) \times 10^2$
Data	463	141	1131	171

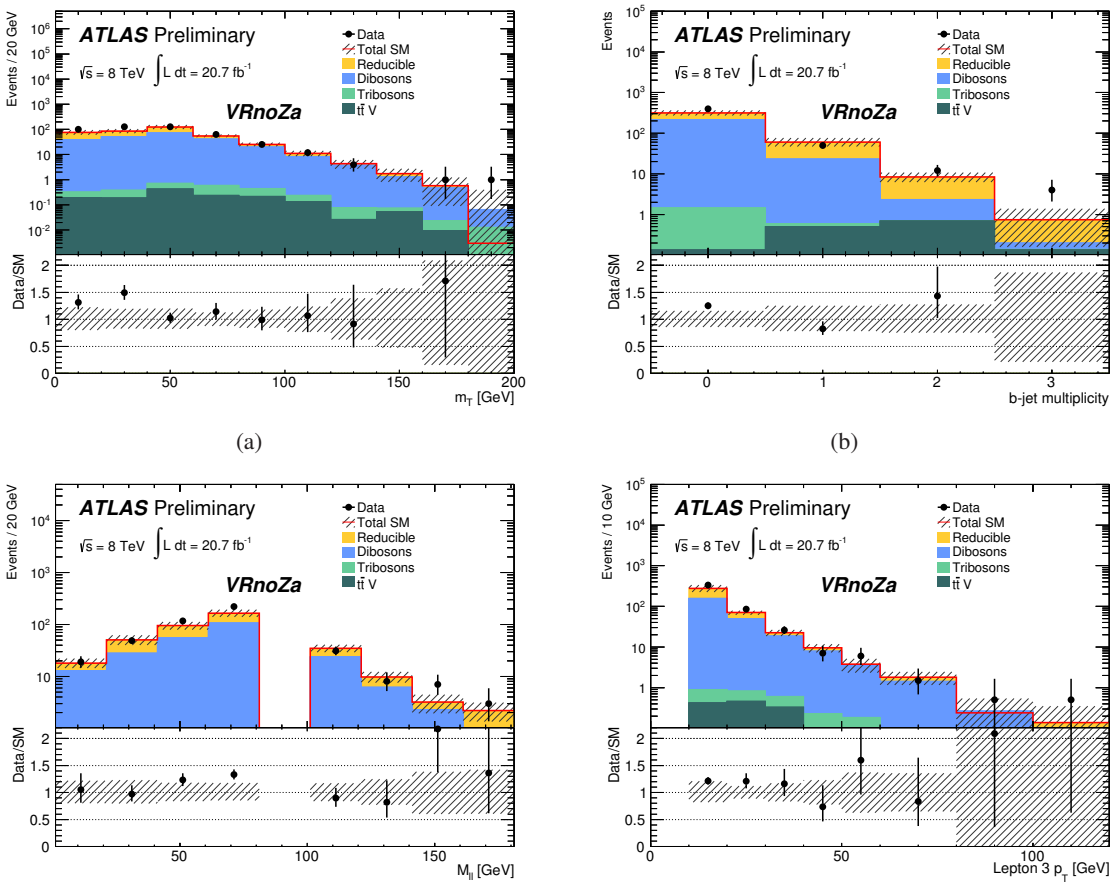

(a) (b)

(c) (d)

Figure 2: For events in VRnoZa the (a) m_{T}, (b) b-jet multiplicity, (c) m_{SFOS} and (d) third lepton p_{T} distributions are shown. The uncertainty band includes both statistical and systematic uncertainties on the SM prediction. The last bin in each distribution does not include the overflow.

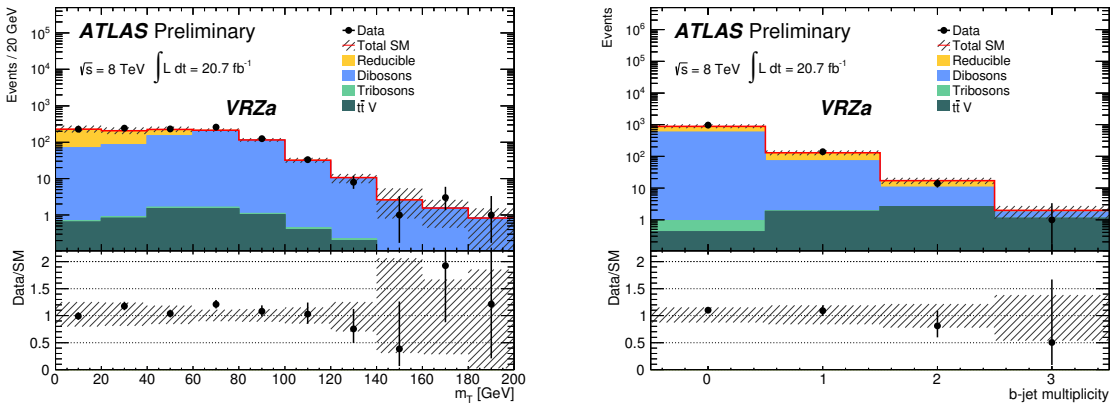

(a) (b)

Figure 3: For events in VRZa the (a) m_{T} and (b) b-jet multiplicity distributions are shown. The uncertainty band includes both statistical and systematic uncertainties on the SM prediction. The last bin in each distribution does not include the overflow.

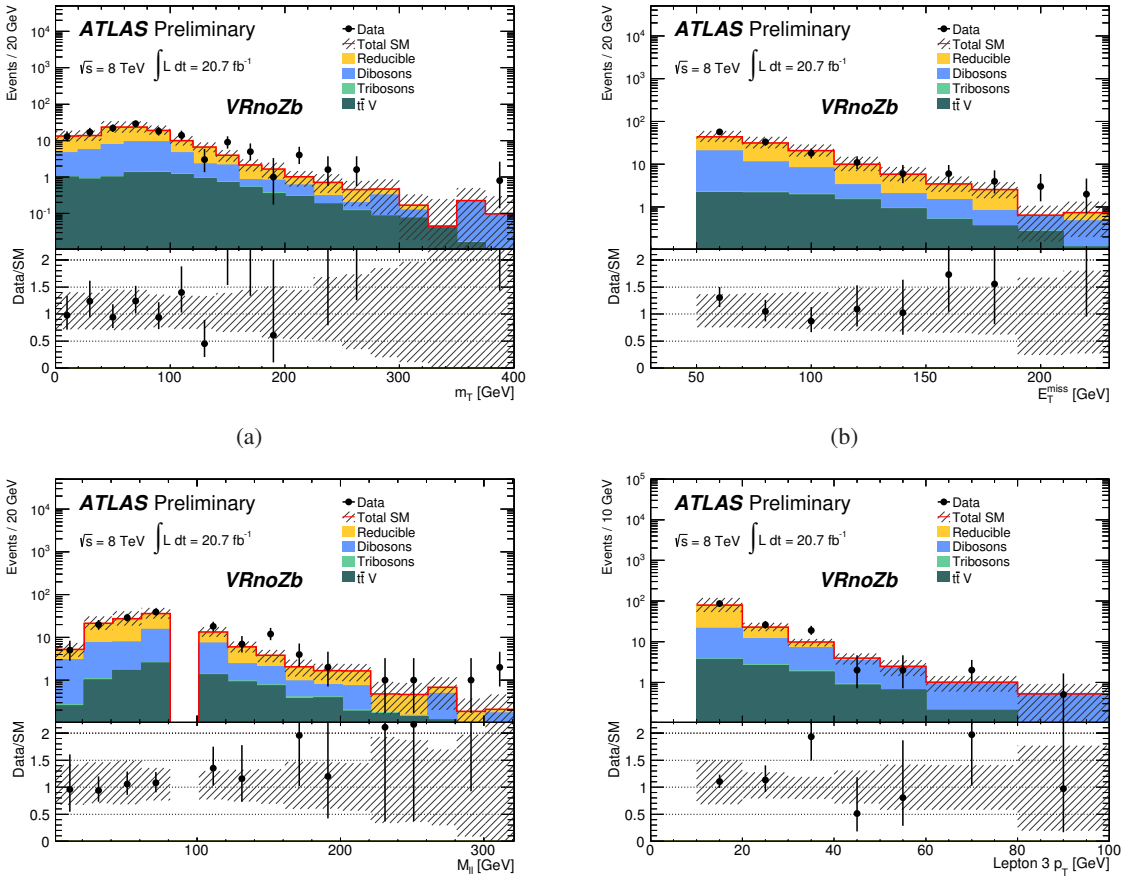

(a) (b)

(c) (d)

Figure 4: For events in VRnoZb the (a) m_{T}, (b) $E_{\mathrm{T}}^{\mathrm{miss}}$, (c) m_{SFOS}, and (d) the third lepton p_{T} distributions are shown. The uncertainty band includes both statistical and systematic uncertainties on the SM prediction. The last bin in each distribution does not include the overflow.

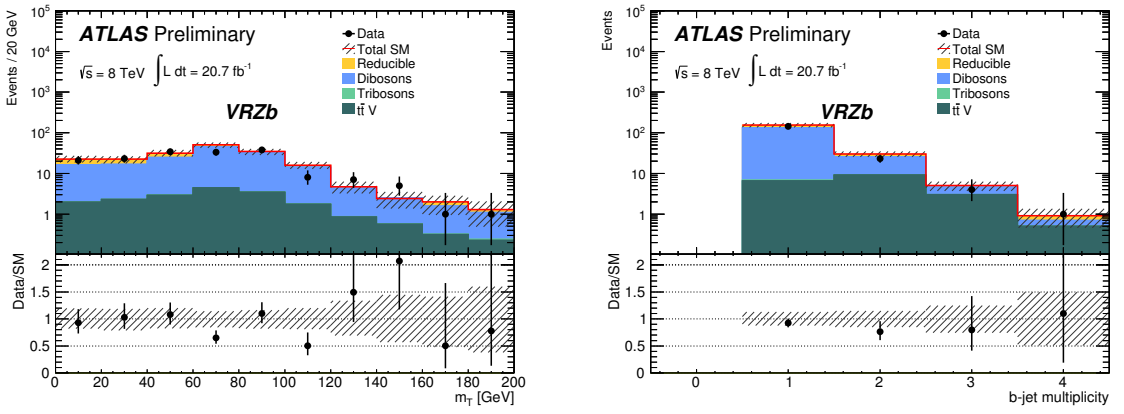

(a) (b)

Figure 5: For events in VRZb the (a) m_{T} and (b) b-jet multiplicity distributions are shown. The uncertainty band includes both statistical and systematic uncertainties on the SM prediction. The last bin in each distribution does not include the overflow.

9 Results and Interpretation

The numbers of observed events and the prediction for SM backgrounds in the six signal regions are given in Table 4. Distributions of the missing transverse energy and the transverse mass in the signal regions are presented in Figures 6 and 7.

Table 4: Expected numbers of events from SM backgrounds and observed numbers of events in data in the signal regions, for 20.7 fb^{-1}. Both statistical and systematic uncertainties are included. The discovery p_0-value of the background only hypothesis is shown. The number of signal events N_{signal} and visible cross-section σ_{visible} that can be excluded with 95% CL are also shown.

Selection	SRnoZa	SRnoZb	SRnoZc	SRZa	SRZb	SRZc
Tri-boson	1.7 ± 1.7	0.6 ± 0.6	0.8 ± 0.8	0.5 ± 0.5	0.4 ± 0.4	0.29 ± 0.29
ZZ	14 ± 8	1.8 ± 1.0	0.25 ± 0.17	8.9 ± 1.8	1.0 ± 0.4	0.39 ± 0.28
$t\bar{t}V$	0.23 ± 0.23	0.21 ± 0.19	$0.21^{+0.30}_{-0.21}$	0.4 ± 0.4	0.22 ± 0.21	0.10 ± 0.10
WZ	50 ± 9	20 ± 4	2.1 ± 1.6	235 ± 35	19 ± 5	5.0 ± 1.4
Σ SM irreducible	65 ± 12	22 ± 4	3.4 ± 1.8	245 ± 35	20 ± 5	5.8 ± 1.4
SM reducible	31 ± 14	7 ± 5	1.0 ± 0.4	4^{+5}_{-4}	1.7 ± 0.7	0.5 ± 0.4
Σ SM	$\mathbf{96 \pm 19}$	$\mathbf{29 \pm 6}$	$\mathbf{4.4 \pm 1.8}$	$\mathbf{249 \pm 35}$	$\mathbf{22 \pm 5}$	$\mathbf{6.3 \pm 1.5}$
Data	**101**	**32**	**5**	**273**	**23**	**6**
p_0-value	0.41	0.37	0.40	0.23	0.44	0.5
N_{signal} excluded (exp)	39.3	16.3	6.2	67.9	13.2	6.7
N_{signal} excluded (obs)	41.8	18.0	6.8	83.7	13.9	6.5
σ_{visible} excluded (exp) [fb]	1.90	0.79	0.30	3.28	0.64	0.32
σ_{visible} excluded (obs) [fb]	2.02	0.87	0.33	4.04	0.67	0.31

No significant excess of events is found in any of the six signal regions. Upper limits on the visible cross-section, defined as the production cross-section times acceptance times efficiency, are placed at 95% CL with the CL_s prescription [63] for each signal region (Table 4). All systematic uncertainties and their correlations are taken into account via nuisance parameters in a profile likelihood fit [64].

For each of the SUSY model points, the limit is calculated using a combined likelihood of all the signal regions. For the exclusion limits shown in this section, the expected and observed limits are calculated for each SUSY model point, taking into account the theoretical and experimental uncertainties on the SM background and the experimental uncertainties on the signal. The impact of the uncertainties on the signal cross-section is also shown for the observed limit only.

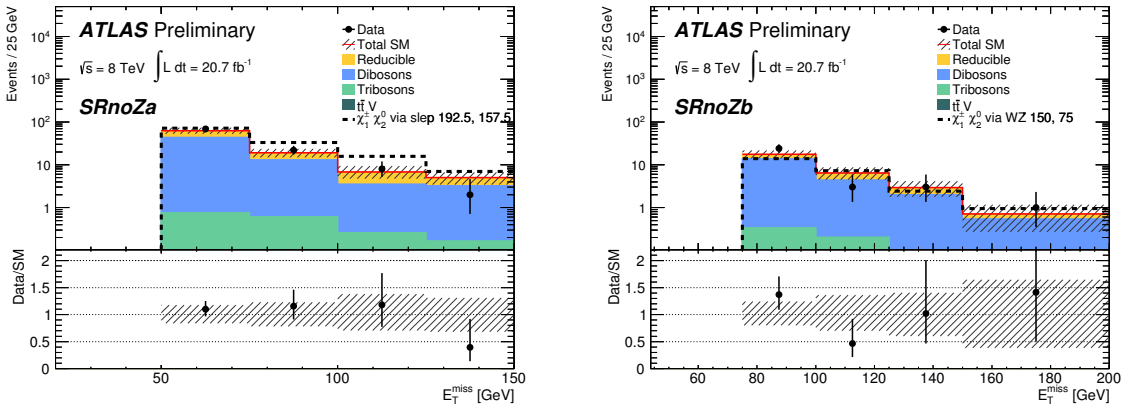

(a) SRnoZa

(b) SRnoZb

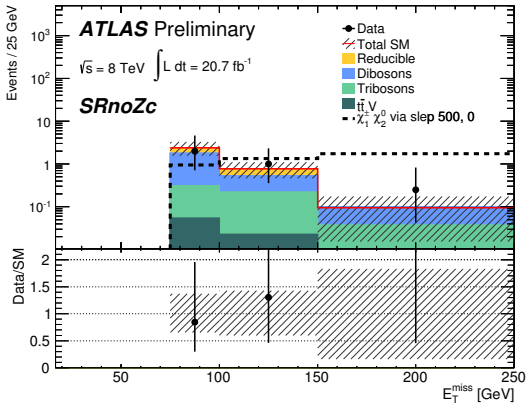

(c) SRnoZc

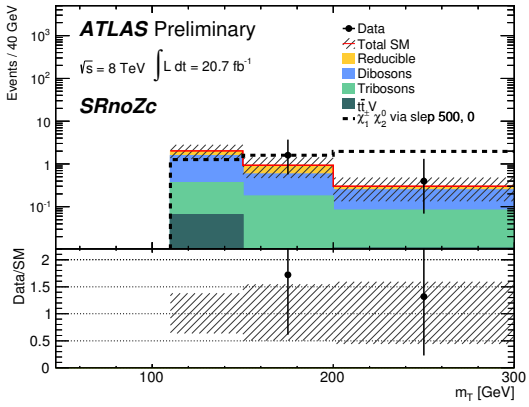

(d) SRnoZc

Figure 6: The $E_{\mathrm{T}}^{\mathrm{miss}}$ distributions for events in signal regions (a) SRnoZa, (b) SRnoZb, (c) SRnoZc, as well as (d) the m_{T} distribution in SRnoZc are shown. The uncertainty band includes both statistical and systematic uncertainty, while the uncertainties on the data points are statistical only. The yields of simplified model scenarios are also shown for illustration purposes, where "$\tilde{\chi}_1^{\pm}\tilde{\chi}_2^0$ via slep x,y" ("$\tilde{\chi}_1^{\pm}\tilde{\chi}_2^0$ via WZ x,y") are scenarios from the simplified models with decays via sleptons (via gauge bosons), and x is the $\tilde{\chi}_2^0$, $\tilde{\chi}_1^{\pm}$ mass and y is the $\tilde{\chi}_1^0$ mass in GeV. The SUSY scenarios shown here produce negligible contamination in the validation regions. The signal distributions are not stacked on top of the expected background. The last bin in each distribution does not include the overflow.

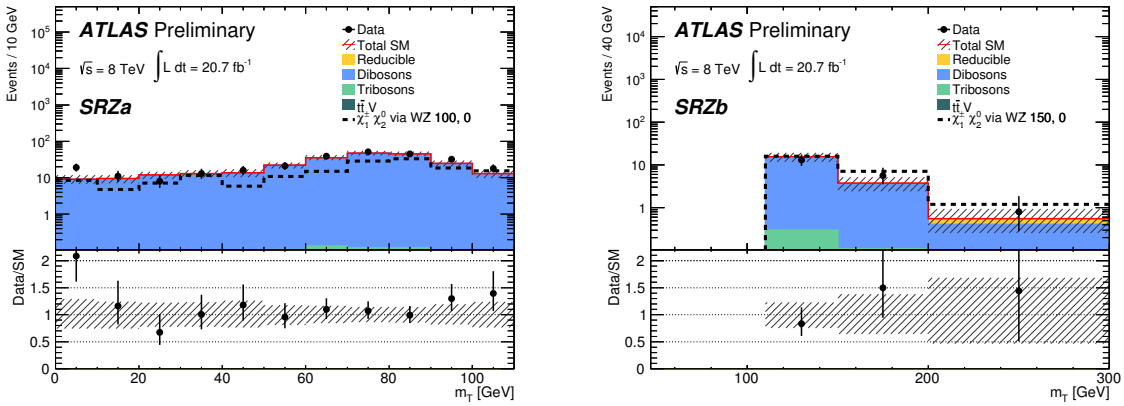

(a) SRZa

(b) SRZb

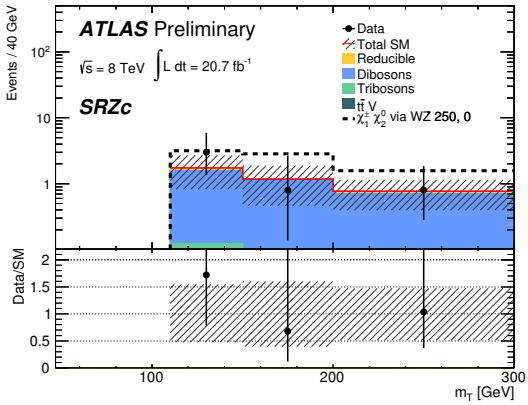

(c) SRZc

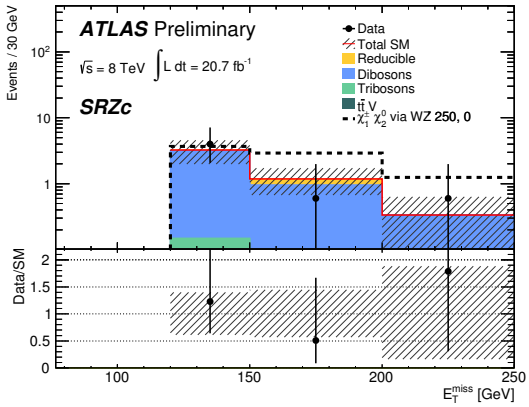

(d) SRZc

Figure 7: The m_{T} distributions for events in signal regions (a) SRZa, (b) SRZb, (c) SRZc, as well as (d) the $E_{\mathrm{T}}^{\mathrm{miss}}$ distribution in SRZc are shown. The uncertainty band includes both statistical and systematic uncertainty, while the uncertainties on the data points are statistical only. The yields of simplified model scenarios are also shown for illustration purposes, where "$\tilde{\chi}_1^{\pm}\tilde{\chi}_2^0$ via slep x,y" ("$\tilde{\chi}_1^{\pm}\tilde{\chi}_2^0$ via WZ x,y") are scenarios from the simplified models with decays via sleptons (via gauge bosons), and x is the $\tilde{\chi}_2^0$, $\tilde{\chi}_1^{\pm}$ mass and y is the $\tilde{\chi}_1^0$ mass in GeV. The SUSY scenarios shown here produce negligible contamination in the validation regions. The signal distributions are not stacked on top of the expected background. The last bin in each distribution does not include the overflow.

Regions SRnoZa, SRnoZb and SRnoZc provide the best sensitivity to the simplified models with intermediate slepton decays for which the interpretation is shown in Figure 8(a). In these models, degenerate $\tilde{\chi}_1^\pm$ and $\tilde{\chi}_2^0$ masses up to 600 GeV are excluded for large mass differences with the $\tilde{\chi}_1^0$.

The limit in the simplified model with charginos and neutralinos decaying via gauge bosons is shown in Figure 8(b). The signal region SRnoZa has the best sensitivity for small mass differences between the two lightest neutralinos, which corresponds to the area close to the diagonal. The signal regions SRnoZb, SRZa/b/c are sensitive to the area close to the $m_{\tilde{\chi}_2^0} - m_{\tilde{\chi}_1^0} = m_Z$ line. Finally, SRZa, SRZb and SRZc are sensitive to decays of $\tilde{\chi}_2^0$ into on-mass-shell Z-bosons with high $E_{\mathrm{T}}^{\mathrm{miss}}$, which corresponds to the area far from the diagonal. In these models, degenerate $\tilde{\chi}_1^\pm$ and $\tilde{\chi}_2^0$ masses up to 315 GeV are excluded for large mass differences with the $\tilde{\chi}_1^0$.

In scenarios with gauge coupling unification, the $m_{\tilde{\chi}_2^0} = 2m_{\tilde{\chi}_1^0}$ relationship is expected to nearly hold. This constraint is indicated in the plots of Figure 8. Under this assumption, degenerate $\tilde{\chi}_1^\pm$ and $\tilde{\chi}_2^0$ masses of up to ~580 (170) GeV are excluded when they decay via sleptons (via gauge bosons).

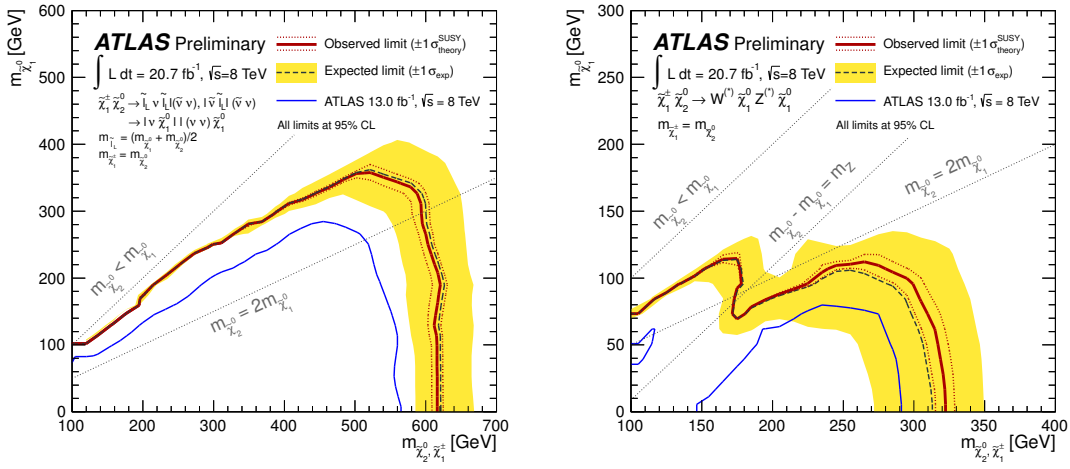

(a) Decay via sleptons

(b) Decay via gauge bosons

Figure 8: Observed and expected 95% CL limit contours for chargino and neutralino production in the simplified model scenario with (a) decay via sleptons and (b) decay via gauge bosons. The band around the median expected limit shows the $\pm 1\sigma$ variations on the median expected limit, including all uncertainties except theoretical uncertainties on the signal cross-section. The dotted lines around the observed limit indicate the sensitivity to $\pm 1\sigma$ variations on these theoretical uncertainties. The blue lines correspond to the 8 TeV, 13 fb^{-1} limits from the ATLAS three lepton analysis [18]. The limits are calculated using the statistical combination of all signal regions for each of the model points. Linear interpolation is used to account for the discrete nature of the signal grids.

10 Summary

Results from a search for direct production of charginos and neutralinos in the final state with three leptons (electrons or muons) and missing transverse momentum are reported. The analysis is based on 20.7 fb^{-1} of proton-proton collision data recorded by ATLAS at $\sqrt{s}$ =8 TeV. No significant excess of events is found in data above SM expectations. The null result is interpreted in simplified SUSY models. For the simplified SUSY models with intermediate slepton decays, degenerate $\tilde{\chi}_1^\pm$ and $\tilde{\chi}_2^0$ masses up to

600 GeV are excluded for large mass differences with the $\tilde{\chi}_1^0$. For the simplified SUSY models with gauge boson decays, degenerate $\tilde{\chi}_1^\pm$ and $\tilde{\chi}_2^0$ masses up to 315 GeV are excluded for large mass differences with the $\tilde{\chi}_1^0$.

References

[1] H. Miyazawa, Prog. Theor. Phys. **36 (6)** (1966) 1266–1276.

[2] P. Ramond, Phys. Rev. **D 3** (1971) 2415–2418.

[3] Y. A. Gol'fand and E. P. Likhtman, JETP Lett. **13** (1971) 323–326.

[4] A. Neveu and J. H. Schwarz, Nucl. Phys. **B 31** (1971) 86–112.

[5] A. Neveu and J. H. Schwarz, Phys. Rev. **D 4** (1971) 1109–1111.

[6] J. Gervais and B. Sakita, Nucl. Phys. **B 34** (1971) 632–639.

[7] D. V. Volkov and V. P. Akulov, Phys. Lett. **B 46** (1973) 109–110.

[8] J. Wess and B. Zumino, Phys. Lett. **B 49** (1974) 52.

[9] J. Wess and B. Zumino, Nucl. Phys. **B 70** (1974) 39–50.

[10] P. Fayet, Phys. Lett. **B 64** (1976) 159.

[11] P. Fayet, Phys. Lett. **B 69** (1977) 489.

[12] G. R. Farrar and P. Fayet, Phys. Lett. **B 76** (1978) 575–579.

[13] P. Fayet, Phys. Lett. **B 84** (1979) 416.

[14] S. Dimopoulos and H. Georgi, Nucl. Phys. **B 193** (1981) 150.

[15] R. Barbieri and G. Giudice, Nucl. Phys. **B 306** (1988) 63.

[16] B. de Carlos and J. Casas, Phys. Lett. **B 309** (1993) 320–328, arXiv:hep-ph/9303291.

[17] J. Alwall et al., Phys. Rev. **D 79** (2009) 075020, arXiv:0810.3921 [hep-ph].

[18] ATLAS Collaboration, ATLAS-CONF-2012-154. http://cdsweb.cern.ch/record/1493493.

[19] ATLAS Collaboration, arXiv:1208.3144 [hep-ex].

[20] ATLAS Collaboration, arXiv:1208.2884 [hep-ex].

[21] ATLAS Collaboration, Phys. Rev. Lett. **108** (2012) 261804, arXiv:1204.5638 [hep-ex].

[22] CMS Collaboration, arXiv:1209.6620 [hep-ex].

[23] D0 Collaboration, V. Abazov et al., Phys. Lett. **B 680** (2009) 34–43, arXiv:0901.0646 [hep-ex].

[24] CDF Collaboration, T. Aaltonen et al., Phys. Rev. Lett. **101** (2008) 251801, arXiv:0808.2446 [hep-ex].

[25] LEPSUSYWG, ALEPH, DELPHI, L3, OPAL Collaborations, LEPSUSYWG/01-03.1 (2001). http://lepsusy.web.cern.ch/lepsusy/www/inos_moriond01/charginos_pub.html.

[26] ATLAS Collaboration, JINST **3** (2008) S08003.

[27] ATLAS Collaboration, arXiv:0901.0512 [hep-ex].

[28] T. Gleisberg et al., JHEP **0902** (2009) 007, arXiv:0811.4622 [hep-ph].

[29] M. L. Mangano et al., JHEP **0307** (2003) 001, arXiv:hep-ph/0206293.

[30] J. Alwall et al., JHEP **0709** (2007) 028, arXiv:0706.2334 [hep-ph].

[31] P. Nason, JHEP **0411** (2004) 040, arXiv:hep-ph/0409146.

[32] B. P. Kersevan and E. Richter-Was, Comput. Phys. Commun. **149** (2003) 142–194, arXiv:hep-ph/0201302 [hep-ph].

[33] S. Frixione and B. R. Webber, arXiv:hep-ph/0601192.

[34] P. M. Nadolsky et al., Phys. Rev. **D 78** (2008) 013004, arXiv:0802.0007 [hep-ph].

[35] H.-L. Lai et al., Phys. Rev. **D 82** (2010) 074024, arXiv:1007.2241 [hep-ph].

[36] G. Corcella et al., JHEP **0101** (2001) 010, arXiv:hep-ph/0011363.

[37] T. Sjöstrand et al., JHEP **0605** (2006) 026, arXiv:hep-ph/0603175 [hep-ph].

[38] J. Butterworth et al., Z. Phys. **C 72** (1996) 637–646, arXiv:hep-ph/9601371 [hep-ph].

[39] GEANT4 Collaboration, Nucl. Instrum. Meth. **A 506** (2003) 250–303.

[40] ATLAS Collaboration, Eur. Phys. J. **C 70** (2010) 823–874, arXiv:1005.4568 [physics.ins-det].

[41] ATLAS Collaboration, ATL-PHYS-PUB-2010-013. https://cdsweb.cern.ch/record/1300517.

[42] J. M. Campbell and R. K. Ellis, Phys. Rev. **D 60** (1999) 113006, arXiv:hep-ph/9905386 [hep-ph].

[43] J. M. Campbell et al., JHEP **1107** (2011) 018, arXiv:1105.0020 [hep-ph].

[44] F. Campanario et al., Phys. Rev. **D 78** (2008) 094012, arXiv:0809.0790 [hep-ph].

[45] M. Aliev et al., Comput. Phys. Commun. **182** (2011) 1034–1046, arXiv:1007.1327 [hep-ph].

[46] A. Kardos et al., Phys. Rev. **D 85** (2012) 054015, arXiv:1111.0610 [hep-ph].

[47] J. M. Campbell and R. K. Ellis, JHEP **1207** (2012) 052, arXiv:1204.5678 [hep-ph].

[48] S. Catani et al., Phys. Rev. Lett. **103** (2009) 082001, arXiv:0903.2120 [hep-ph].

[49] A. Martin et al., Eur. Phys. J. **C 63** (2009) 189–285, arXiv:0901.0002 [hep-ph].

[50] M. Bähr et al., Eur. Phys. J. **C 58** (2008) 639–707, arXiv:0803.0883 [hep-ph].

[51] W. Beenakker et al., Nucl. Phys. **B 492** (1997) 51–103, arXiv:hep-ph/9610490.

[52] M. Krämer et al., arXiv:1206.2892 [hep-ph].

[53] ATLAS Collaboration, Eur. Phys. J. **C 72** (2012) 1909, arXiv:1110.3174 [hep-ex].

[54] ATLAS Collaboration, JHEP **1012** (2010) 060, arXiv:1010.2130 [hep-ex].

[55] M. Cacciari et al., JHEP **0804** (2008) 063, arXiv:0802.1189 [hep-ph].

[56] ATLAS Collaboration, ATL-LARG-PUB-2008-002. http://cdsweb.cern.ch/record/1099735.

[57] ATLAS Collaboration, Eur. Phys. J. **C 73** (2013) 2304, arXiv:1112.6426 [hep-ex].

[58] ATLAS Collaboration, ATLAS-CONF-2011-102. http://cdsweb.cern.ch/record/1369219.

[59] ATLAS Collaboration, ATLAS-CONF-2012-043. http://cdsweb.cern.ch/record/1435197.

[60] ATLAS Collaboration, Eur. Phys. J. **C 71** (2011) 1577, arXiv:1012.1792 [hep-ex].

[61] ATLAS Collaboration, Eur. Phys. J. **C72** (2012) 2173, arXiv:1208.1390 [hep-ex].

[62] ATLAS Collaboration, submitted to EPJC, arXiv:1302.4393 [hep-ex].

[63] A. L. Read, J. Phys. G **28** (2002) 2693.

[64] G. Cowan et al., Eur. Phys. J C **71** (2011) 1–19.

A Cut flow for selected benchmark points

Table 5: Expected number of events from representative SUSY signal models in the signal regions with high sensitivity. The decay modes of the charginos and neutralinos is indicated as well as the their masses and production cross-sections. The number of events expected for a luminosity of 20.7 fb^{-1} is quoted at each step of the selection.

Model	Simplified	Simplified	Simplified	Simplified	Simplified	Simplified
Decay via	$\tilde{\ell}_{\text{L}}$	WZ	$\tilde{\ell}_{\text{L}}$	WZ	WZ	WZ
$m_{\tilde{\chi}_1^0}$, $m_{\tilde{\chi}_2^0}$ [GeV]	157.5, 192.5	75, 150	0, 500	0, 100	0, 150	0, 250
$\sigma(pp \to \tilde{\chi}_1^{\pm}\tilde{\chi}_2^0)$ [pb]	0.83 ± 0.05	2.19 ± 0.14	0.0111 ± 0.0009	10.2 ± 0.8	2.19 ± 0.14	0.288 ± 0.018
Signal Region	SRnoZa	SRnoZb	SRnoZc	SRZa	SRZb	SRZc
Generated events (raw)	25000	20000	40000	15000	20000	20000
Events after selection cuts (weighted and normalised to 20.7 fb^{-1})						
Lepton multiplicity	537.1	227.3	28.5	1071.4	259.8	40.0
SFOS requirement	536.3	226.5	28.1	1067.5	258.0	39.7
b veto	491.0	211.0	24.9	989.4	240.0	36.4
Z veto/request	476.3	196.6	24.1	912.7	227.1	34.4
$E_{\text{T}}^{\text{miss}}$	161.2	53.8	22.1	170.7	67.7	17.7
m_{SFOS}	141.2	27.1	–	–	–	–
m_{T}	–	–	19.2	159.3	27.8	12.0
p_{T} 3$^{\text{rd}}$ ℓ	–	–	18.4	–	–	–
SRnoZc veto	141.2	26.3	–	–	–	–

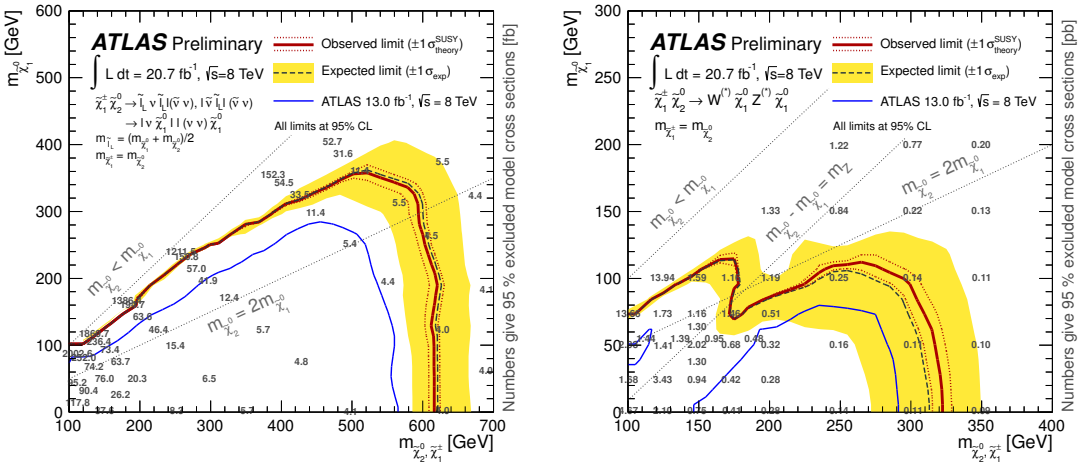

(a) (b)

Figure 9: Observed and expected 95% CL limit contours for chargino and neutralino production in the simplified model scenario with (a) decay via sleptons and (b) decay via gauge bosons. The band around the median expected limit shows the $\pm 1\sigma$ variations on the median expected limit, including all uncertainties except theoretical uncertainties on the signal cross-section. The dotted lines around the observed limit indicate the sensitivity to $\pm 1\sigma$ variations on these theoretical uncertainties. The blue lines correspond to the 8 TeV, 13 fb^{-1} limits from the ATLAS three lepton analysis [18]. The limits are calculated using the statistical combination of all signal regions for each of the model points. Linear interpolation is used to account for the discrete nature of the signal grids. The overlaid numbers give the observed upper limit on the signal cross-section.